RSC Advances

PAPER

View Article Online
View Journal | View Issue

Cite this: *RSC Adv.*, 2025, **15**, 46297

Fluorescent solvatochromism and nonfluorescence processes of charge-transfer-type molecules with a 4-nitrophenyl moiety

Marino Miwa[a] and Akitaka Ito *[ab]

A novel naphthalene derivative, 1-methoxy-4-(4-nitrophenyl)naphthalene (**1**), exhibited obvious fluorescence, the color of which varied significantly from greenish blue to red depending on the solvent, from the charge-transfer excited state with a large electric dipole moment. The fluorescence of **1** was weak in both low- and high-polar solvents, and the fluorescence of derivatives with a 4-nitrophenyl group was also weak in low-polar solvents. Such unusual solvent dependences were revealed by the energy gap plot. The high-energy fluorescent excited state of a derivative with the 4-nitrophenyl group is quickly converted into the triplet excited state, whereas the low-energy state deactivates to the ground state through internal conversion. Such nonfluorescence processes of the derivatives were elucidated by developing derivatives with a nitro group that exhibited fluorescence changes in the broad visible region depending on the chemical structure and solvent.

Received 27th September 2025
Accepted 10th November 2025

DOI: 10.1039/d5ra07359f

rsc.li/rsc-advances

Introduction

Fluorescent organic compounds are utilized in a variety of photochemical applications, such as organic light-emitting diodes[1,2] and bioimaging.[3,4] In particular, compounds exhibiting fluorescence color changes depending on the solvent (so-called fluorescent solvatochromism) are fascinating targets that can be used as chemical sensors to visualize the surrounding environment.[5–8] Fluorescent solvatochromism phenomena are typically induced by solvation of a solute in the excited state.[6] In a solvent that greatly stabilizes the excited state of a solute, the fluorescence is lowered in energy. Since a clear and general solvation process originates from dipole interactions, molecular designs that induce a significant change in the electronic configuration between the ground and excited states, specifically those resulting in a large electric dipole moment (defined as the product of charge and displacement vector) in the excited state, are crucial. A large electric dipole moment in the excited state can be achieved through an electronic transition with a charge-transfer character by introducing strong electron-donating and/or -withdrawing groups, particularly at the periphery of large π-electron systems.

Herein, we focused on the use of a nitro group as a substituent in charge-transfer compounds. This moiety exhibits strong electron-withdrawing ability (Hammett constant σ_p = +0.78) through both resonance and inductive effects.[9] For example, the introduction of a nitro group can reduce the electron density and enhance the oxidizing ability of a compound. In practice, an electron-deficient pyridinium with nitro groups has been reported to act as an excellent oxidative quencher in a photoinduced electron–transfer reaction.[10] Owing to this strong electron-withdrawing ability, the nitro group is a possible candidate to extend the charge-transfer character of a molecule. Most compounds with a nitro group are, however, nonemissive owing to the fast intersystem crossing, internal conversion and so forth.[11,12] Especially, charge-transfer excited states of derivatives with a nitro group(s) are often classified as nonemissive states. Konishi and coworkers reported fluorescent compounds with a nitro group(s).[13] In their report, 2-methoxy-6-(4-nitrophenyl)naphthalene exhibited fluorescent solvatochromism, as predicted by the strong electron-withdrawing ability. Although an appropriate molecular design with a nitro group can yield attractive fluorescent compounds, the number of reports on fluorescent compounds with a nitro group(s) is still limited, and the origin of the reduced fluorescence of such compounds, especially with a charge-transfer excited state(s), is not necessarily clear at this stage. Thus, the development of fluorescent compounds with a nitro group(s) and an increased understanding of the nonfluorescence pathway(s) based on detailed photophysical characterizations of the compounds are among the most important topics for the future design of fluorescent compounds.

In this study, we designed and synthesized a novel naphthalene derivative with a 4-nitrophenyl moiety and a methoxy group at the 1- and 4-positions (**1**). Derivative **1** is an isomer of 2-methoxy-6-(4-nitrophenyl)naphthalene reported by Konishi and

[a]*Graduate School of Engineering, Kochi University of Technology, Miyanokuchi 185, Tosayamada, Kami, Kochi 782-8502, Japan*

[b]*Research Center for Advanced Chiral Optical Materials (RACOMs), Research Institute, Kochi University of Technology, Miyanokuchi 185, Tosayamada, Kami, Kochi 782-8502, Japan. E-mail: ito.akitaka@kochi-tech.ac.jp*

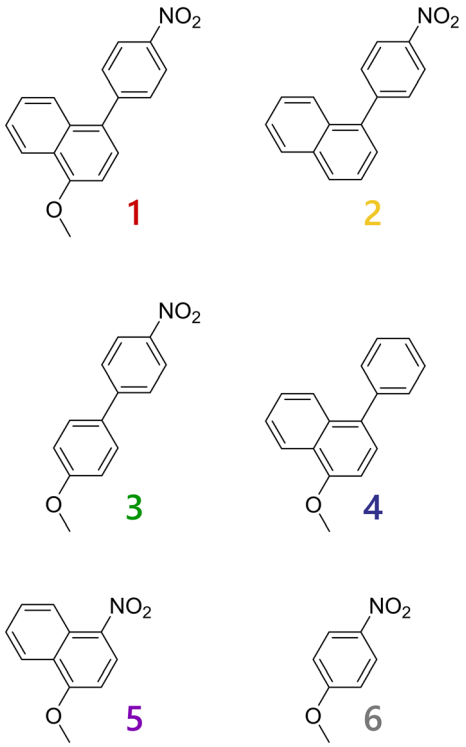

Scheme 1 Chemical structures of **1**–**6**.

coworkers. Since the electron-withdrawing nitro and electron-donating methoxy groups in **1 are introduced in a linear arrangement**, efficient coupling between the transition dipoles arising from the substituents and the large electric dipole moment in its excited state is expected. In practice, **1** exhibited large fluorescent solvatochromism ranging from greenish blue to red. The spectroscopic and photophysical properties of **1** were investigated in detail by comparing reference derivatives, **2** and **4**, without the methoxy and nitro groups, respectively, and **3**, **5** and **6**, with varied crosslinking structures between the substituents (Scheme 1). On the basis of comprehensive photophysical characterizations for the derivatives, we also succeeded in modeling nonfluorescence processes of compounds with a 4-nitrophenyl group.

Experimental

Synthesis and characterization

Reagents purchased from Fujifilm Wako Pure Chemical Corporation, Tokyo Chemical Industry Co., Ltd, or Nacalai Tesque, Inc., were used for the synthesis as supplied. The obtained materials were purified by column chromatography using silica gel 60 (particle size: 63–210 μm, Kanto Chemical Co., Inc.). Thin-layer chromatography was performed with silica gel 60 F_{254}, neutral, on aluminum sheets (Merck Millipore), and spots were visualized with an ASONE SLUV-6 handy UV lamp. Melting points of the compounds were determined using an MPA100 melting point apparatus (Stanford Research Systems). ^{1}H NMR spectra in $CDCl_3$ (NMR grade, Kanto Chemical Co., Inc.) were recorded on a JEOL JMN-ECZ400S spectrometer (399.78 MHz). Chemical shifts of the spectra are given in ppm with tetramethylsilane as an internal standard (0.00 ppm). Atmospheric pressure chemical ionization mass spectrometry (APCI-MS) was performed by direct injection into the mass detector of a Bruker compact QTOF system. Infrared (IR) diffuse reflectance spectra of the compounds diluted in potassium bromide (KBr) were recorded on a Jasco FT/IR-4600 Fourier-transform infrared spectrometer.

A crystal of **1**, **4** or **5** was picked up under an optical microscope, and single-crystal XRD measurements were performed using a Rigaku XtaLAB Synergy-S/Mo system (Mo Kα, λ = 0.71073 Å). X-ray diffraction data were collected at 93 or 103 K with a HyPix-600HE photon counting detector and analyzed using the Olex2 crystallographic software package.[14] The structure was solved by direct methods (ShelXT[15]) and refined through full-matrix least-squares techniques on F^2 using ShelXL.[16] All non-hydrogen atoms were refined with anisotropic displacement parameters. Hydrogen atoms were placed at calculated positions and refined "riding" on their corresponding carbon, nitrogen or oxygen atoms.

Synthesis of 1-methoxy-4-(4-nitrophenyl)naphthalene (1). Synthesis was performed with minor changes in the reported procedure.[17] To a solution of 1-bromo-4-methoxynaphthalene (0.16 mL, 1.0 mmol) and 4-nitrophenylboronic acid (0.25 g, 1.5 mmol) in a toluene/ethanol mixture (16 mL/6 mL) in a three-necked round-bottom flask, an aqueous solution of sodium carbonate (2.1 M (= mol dm^{-3}), 8 mL) was added. The biphasic mixture was deaerated by bubbling for 15 min with argon gas at ambient temperature. Tetrakis(triphenylphosphine)palladium(0) ([Pd(PPh_3)$_4$], 0.05 g, 0.05 mmol) was added, then the mixture was refluxed for 15 h. After cooling to ambient temperature, water (100 mL) was added, and products were extracted with dichloromethane (4 × 100 mL). The combined organic layer was washed with brine (300 mL), dried over anhydrous $MgSO_4$, and evaporated under reduced pressure. Purification by two column chromatography runs (*n*-hexane/dichloromethane = 3/2 (v/v) and *n*-hexane/dichloromethane = 1/1 (v/v)) followed by recrystallization from ethanol afforded **1** as yellow blocks (0.06 g, 22%). R_f = 0.35 (*n*-hexane/dichloromethane = 1/1 (v/v)); m.p. 175.4–178.0 °C; ^{1}H NMR ($CDCl_3$): δ = 8.38 (dd, ^{1}H, J = 2.2, 8.2 Hz, 5-Ar–H of Naph), 8.34 (td, 2H, J = 2.3, 9.1 Hz, 3- and 5-Ar–H of Ph), 7.77 (dd, ^{1}H, J = 1.4, 7.4 Hz, 8-Ar–H of Naph), 7.65 (td, 2H, J = 2.0, 9.0 Hz, 2- and 6-Ar–H of Ph), 7.53 (ddd, ^{1}H, J = 1.3, 6.7, 8.0 Hz, 6- or 7-Ar–H of Naph), 7.49 (ddd, ^{1}H, J = 1.4, 6.6, 7.8 Hz, 6- or 7-Ar–H of Naph), 7.36 (d, ^{1}H, J = 8.0 Hz, 3-Ar–H of Naph), 6.90 (d, ^{1}H, J = 8.0 Hz, 2-Ar–H of Naph), 4.07 ppm (s, 3H, OCH_3); HRMS (APCI, positive mode): *m*/*z* calcd. for [M + H]$^+$: 280.0968; found: 280.0980; IR (KBr): $\tilde{\nu}$ = 3072 (Ar), 3007 (Ar), 2966 (Ar), 2940 (CH_3), 2842 (CH_3), 1582 (Ar), 1512 (NO_2), 1463 (Ar), 1342 (NO_2), 1239 (C–O–C), 1110 (Ar), 1156 (Ar), 1081 (Ar), 1026 (C–O–C), 994 (Ar), 863 (Ar–NO_2), 813 (Ar), 770 (Ar), 725 (Ar), 702 cm^{-1} (Ar).

Synthesis of 1-(4-nitrophenyl)naphthalene (2). The reaction was performed as describe for the synthesis of **1** by using 1-bromonaphthalene (0.56 mL, 4.0 mmol), 4-nitrophenylboronic acid (0.87 g, 5.2 mmol), toluene (64 mL), ethanol (24 mL),

aqueous Na_2CO_3 solution (2.0 M, 32 mL) and [$Pd(PPh_3)_4$] (0.15 g, 0.13 mmol). After refluxing for 65 h, water (300 mL) was added, and products were extracted with chloroform (3 × 300 mL). The combined organic layer was washed with brine (500 mL), dried over anhydrous $MgSO_4$, and evaporated under reduced pressure. Purification by column chromatography (*n*-hexane/dichloromethane = 3/2 (v/v)), followed by recrystallization from *n*-hexane, afforded **2** as colorless needles (0.16 g, 16%). R_f = 0.48 (*n*-hexane/dichloromethane = 3/2 (v/v)); m.p. 130.7–133.2 °C; ^{1}H NMR ($CDCl_3$): δ = 8.37 (td, 2H, J = 2.2, 9.0 Hz, 3- and 5-Ar–H of Ph), 7.94 (dd, 2H, J = 3.0, 7.8 Hz, 3-Ar–H of Naph), 7.78 (d, ^{1}H, J = 8.4 Hz, 8-Ar–H of Naph), 7.68 (td, 2H, J = 2.4, 9.2 Hz, 2- and 4-Ar–H of Ph), 7.58–7.52 (m, 2H, 6- or 7-Ar–H and 4-Ar–H of Naph), 7.48 (ddd, ^{1}H, J = 1.4, 7.0, 8.6 Hz, 6- or 7-Ar–H of Naph), 7.42 ppm (dd, ^{1}H, J = 1.2, 7.2 Hz, 2-Ar–H of Naph); HRMS (APCI, positive mode): m/z calcd. for $[M + H]^+$: 250.0863; found: 250.0890; IR (KBr): $\tilde{\nu}$ = 3100 (Ar), 3059 (Ar), 2923 (Ar), 2848 (Ar), 1597 (Ar), 1517 (NO_2), 1397 (Ar), 1349 (NO_2), 1311 (Ar), 1286 (Ar), 1256 (Ar), 1105 (Ar), 1017 (Ar), 961 (Ar), 861 (Ar–NO_2), 804 (Ar), 781 (Ar), 754 (Ar), 700 (Ar), 571 (Ar), 557 cm^{-1} (Ar).

Synthesis of 4-methoxy-4′-nitrobiphenyl (3). The reaction was performed as described for the synthesis of **1** using 1-bromo-4-methoxybenzene (0.37 mL, 3.0 mmol), 4-nitrophenylboronic acid (0.61 g, 3.6 mmol), toluene (48 mL), ethanol (18 mL), aqueous Na_2CO_3 solution (2.1 M, 24 mL) and [$Pd(PPh_3)_4$] (0.15 g, 0.12 mmol). After refluxing for 40 h, water (250 mL) was added, and products were extracted with chloroform (3 × 250 mL). The combined organic layer was washed with brine (500 mL), dried over anhydrous $MgSO_4$, and evaporated under reduced pressure. Purification by two column chromatography runs (*n*-hexane/dichloromethane = 3/2 (v/v) and *n*-hexane/dichloromethane = 4/1 (v/v)), followed by recrystallization from *n*-hexane, afforded **3** as pale-yellow blocks (0.09 g, 13%). R_f = 0.28 (*n*-hexane/dichloromethane = 4/1 (v/v)); m.p. 105.9–109.4 °C; ^{1}H NMR ($CDCl_3$): δ = 7.02 (td, 2H, J = 2.6, 9.4 Hz, 3′- and 5′-Ar–H), 8.27 (td, 2H, J = 2.3, 9.4 Hz, 2,6-Ar–H or 2′,6′-Ar–H), 7.58 (td, 2H, J = 2.5, 9.5 Hz, 2,6-Ar–H or 2′,6′-Ar–H), 7.69 (td, 2H, J = 2.3, 9.1 Hz, 3- and 5-Ar–H), 3.87 ppm (s, 3H, OCH_3); HRMS (APCI, positive mode): m/z calcd. for $[M + H]^+$: 230.0812; found: 230.0841; IR (KBr): 3062 (Ar), 2929 (CH_3), 2835 (CH_3), 1598 (Ar), 1509 (NO_2), 1343 (NO_2), 1253 (C–O–C), 1186 (Ar), 1108 (Ar), 1034 (C–O–C), 1016 (Ar), 859 (Ar–NO_2), 756 (Ar), 723 (Ar), 697 cm^{-1} (Ar).

Synthesis of 1-methoxy-4-phenylnaphthalene (4). The reaction was performed as described for the synthesis of **1** using 1-bromo-4-methoxynaphthalene (0.40 mL, 2.5 mmol), phenylboronic acid (0.38 g, 3.1 mmol), toluene (40 mL), ethanol (15 mL), aqueous Na_2CO_3 solution (2.1 M, 20 mL) and [$Pd(PPh_3)_4$] (0.12 g, 0.10 mmol). After refluxing for 40 h, water (250 mL) was added, and products were extracted with dichloromethane (3 × 250 mL). The combined organic layer was washed with brine (500 mL), dried over anhydrous $MgSO_4$, and evaporated under reduced pressure. Purification by column chromatography (*n*-hexane/dichloromethane = 9/1 (v/v)), followed by recrystallization from *n*-hexane, afforded **4** as colorless needles (0.06 g, 14%). R_f = 0.38 (*n*-hexane/dichloromethane = 9/1 (v/v)); m.p. 87.3–89.5 °C; ^{1}H NMR ($CDCl_3$): δ = 8.34 (dd, ^{1}H, J = 1.2, 8.4 Hz, 5-Ar–H of Naph), 7.86 (dd, ^{1}H, J = 1.2, 8.4 Hz, 8-Ar–H of Naph), 7.57–7.44 (m, 6H, 6- or 7-Ar–H of Naph and Ar–H of Ph), 7.43–7.38 (m, ^{1}H, 6- or 7-Ar–H of Naph), 7.34 (d, ^{1}H, J = 8.0 Hz, 3-Ar–H of Naph), 6.89 (d, ^{1}H, J = 7.6 Hz, 2-Ar–H of Naph), 4.05 ppm (s, 3H, OCH_3); HRMS (APCI, positive mode): m/z calcd. for $[M + H]^+$: 235.1117; found: 235.1159; IR (KBr): 3010 (Ar), 2955 (CH_3), 2840 (CH_3), 1588 (Ar), 1463 (Ar), 1389 (Ar), 1240 (Ar), 1086 (C–O–C), 824 (Ar), 769 (Ar), 704 cm^{-1} (Ar).

Synthesis of 1-methoxy-4-nitronaphthalene (5). The synthesis was performed as described in the reported procedure, with minor changes.[18] In a three-necked round-bottom flask, 1-hydroxy-4-nitronaphthalene (0.99 g, 5.2 mmol), potassium carbonate (1.26 g, 9.1 mmol) and acetone (50 mL) were added. After stirring at ambient temperature under an argon gas atmosphere for 15 min, iodomethane (0.66 mL, 10.5 mmol) was added, and the mixture was refluxed for 4 h. To the mixture at ambient temperature, water (150 mL) was added, and the products were extracted with dichloromethane (3 × 150 mL). The combined organic layer was washed with water (500 mL), dried over anhydrous $MgSO_4$, and evaporated under reduced pressure. Purification by column chromatography (*n*-hexane/dichloromethane = 1/1 (v/v)), followed by recrystallization from *n*-hexane, afforded **5** as yellow needles (0.35 g, 33%). R_f = 0.30 (*n*-hexane/dichloromethane = 3/2 (v/v)); m.p. 84.7–87.6 °C; ^{1}H NMR ($CDCl_3$): δ = 8.79 (d, ^{1}H, J = 8.4 Hz, 8-Ar–H), 8.42 (d, ^{1}H, J = 8.8 Hz, 3-Ar–H), 8.38 (d, ^{1}H, J = 8.4 Hz, 5-Ar–H), 6.83 (d, ^{1}H, J = 8.8 Hz, 2-Ar–H), 7.75 (ddd, ^{1}H, J = 1.6, 7.0, 8.6 Hz, 6- or 7-Ar–H), 7.60 (ddd, ^{1}H, J = 1.2, 7.0, 8.4 Hz, 6- or 7-Ar–H), 4.11 ppm (s, 3H, OCH_3); HRMS (APCI, positive mode): m/z calcd. for $[M + H]^+$: 204.0655; found: 204.0697; IR (KBr): 3115 (Ar), 3022 (Ar), 2976 (Ar), 2941 (CH_3), 2839 (CH_3), 1571 (Ar), 1513 (Ar), 1500 (NO_2), 1462 (Ar), 1426 (Ar), 1311 (NO_2), 1272 (Ar), 1096 (Ar), 1006 (Ar), 826 (Ar–NO_2), 761 (Ar), 639 cm^{-1} (Ar).

Spectroscopic and photophysical measurements

1-Methoxy-4-nitrobenzene (**6**), purchased from Tokyo Chemical Industry Co., Ltd, was purified by column chromatography (*n*-hexane/dichloromethane = 1/1 (v/v)) followed by recrystallization from *n*-hexane. m.p. 53.6–56.8 °C; ^{1}H NMR ($CDCl_3$): δ = 8.21 (td, 2H, J = 2.8, 9.8 Hz, 3- and 5-Ar–H), 6.96 (td, 2H, J = 3.0, 9.6 Hz, 2- and 6-Ar–H), 3.92 ppm (s, 3H, OCH_3); HRMS (APCI, positive mode): m/z calcd. for $[M + H]^+$: 154.0499; found: 154.0518; IR (KBr): 3116 (Ar), 3079 (Ar), 3063 (Ar), 3035 (Ar), 2978 (Ar), 2946 (CH_3), 2841 (CH_3), 1591 (Ar), 1500 (NO_2), 1333 (NO_2), 1266 (C–O–C), 1176 (Ar), 1109 (Ar), 1022 (C–O–C), 862 (Ar), 848 (Ar–NO_2), 751 (Ar), 692 (Ar), 633 (Ar), 617 (Ar), 534 cm^{-1} (Ar).

Solvents for the spectroscopic and photophysical measurements were used without purification. Toluene, 1,4-dioxane, tetrahydrofuran (THF), ethyl acetate, 1,2-dichloroethane, acetone, *N*,*N*-dimethylformamide (DMF) and dimethyl sulfoxide (DMSO) were spectroscopic-grade solvents from Fujifilm Wako Pure Chemical Corporation. Chloroform and acetonitrile were HPLC solvents from Fujifilm Wako Pure Chemical Corporation and Merck Millipore, respectively.

Dichloromethane was a fluorometry-grade solvent from Kanto Chemical Co., Inc.

Absorption spectra were measured with a Hitachi High-Technologies U-3900 spectrophotometer (slit width: 1 nm, scan speed: 120 nm min^{-1}). Fluorescence quantum yields (Φ_f) of **1–3** were determined by the absolute method with a Hamamatsu Photonics Quantaurus-QY Plus C13534-02 (excitation wavelength: 375 nm, averaging: 1000 times). The Φ_f of **4** was determined by the relative method using anthracene, which was purified by column chromatography (*n*-hexane/dichloromethane = 1/4 (v/v)) followed by vacuum sublimation, in ethanol ($\Phi_{f,An} = 0.21$[19]) as a standard, using eqn (1).

$$\Phi_{f,4} = \Phi_{f,An} \times \frac{\int I_4(\tilde{\nu})d\tilde{\nu}/\left(1-10^{-Abs_4}\right)}{\int I_{An}(\tilde{\nu})d\tilde{\nu}/\left(1-10^{-Abs_{An}}\right)} \times \frac{{n_4}^2}{{n_{An}}^2} \quad (1)$$

where $I(\tilde{\nu})$, Abs and n are fluorescence intensity at wavenumber $\tilde{\nu}$ (obtained with a Hitachi High-Technologies F-4500 spectrofluorometer), excitation wavelength (300 or 340 nm), and refractive index of each solution, respectively. The subscripts "**4**" and "An" represent **4** and anthracene, respectively. Refractive indices of solvents were employed as the n values (*i.e.*, n_4 and n_{An}) owing to the low solute concentration ($<10^{-5}$ M). The fluorescence intensity at each wavelength was corrected for the system spectral response so that the vertical axis of the spectrum corresponds to the photon number at each wavelength. In the fluorescence decay measurements, the second harmonics of the femtosecond-pulsed Ti:sapphire laser (380 nm, 1 MHz) from an MKS Instruments Spectra-Physics Tsunami® 3941-M1BB with a 3980 or GWU-UHG-2PSK-W pulse picker/frequency doubler, was used as an excitation light. Fluorescence from a sample was detected with a Hamamatsu Photonics C4334 streak camera equipped with a C5094 spectrograph. The third harmonics of a pulsed Nd:YAG laser (Continuum Surelite™-II, 355 nm, fwhm: ~6 ns, repetition rate: 10 Hz) and a continuum-wave 150-W xenon short arc lamp (Ushio UXL-S158-O) were used as the excitation and probe light source, respectively, for the transient absorption measurements. The probe light, which irradiated the sample in a cuvette perpendicular to the excitation light, passed through the sample and was detected with a gated ICCD (Princeton PI-MAX) or a photomultiplier tube (Hamamatsu R928) equipped with an imaging spectrometer (Acton SpectraPro 2300i). Samples for transient absorption measurements were deaerated by bubbling with argon gas for 30 min. The fluorescence and transient absorption decay profiles were fitted by a convolution method with the instrumental response function obtained by measuring the excitation-light scattering by colloidal silica LUDOX® HS-30 (Sigma-Aldrich Co. LLC). All the spectroscopic and photophysical data were analyzed with OriginPro 2023 software.

Theoretical calculations

Theoretical calculations for derivatives **1–6** were conducted with Gaussian 16 W software (Revision A.03).[20] The ground-state geometries of a molecule were optimized by using the CAM-B3LYP long-range-corrected functional[21] with the 6-311+G(d,p) basis set.[22] No negative frequency was obtained by the identical methodologies, verifying that the optmized geometries represent local minima on the potential energy surface. Time-dependent density functional theory (TD-DFT) calculations were then performed at the CAM-B3LYP/6-311+G(d,p) level to estimate transition energies and oscillator strengths to give the thirty lowest-energy singlet excited states. The geometries in the lowest-energy singlet excited (S_1) states were then optimized by the TD-DFT method, and the transition energies and oscillator strengths of the 3 lowest-energy singlet and triplet excited states were obtained at the CAM-B3LYP/6-311+G(d,p) level. The calculations were carried out in dichloromethane by using the conductor-like polarizable continuum model (CPCM).[23] Calculations for **1** modeled in toluene, THF and acetone were also performed similarly. The Kohn–Sham orbitals were visualized using GaussView 6.0.16.[24]

Results and discussion

Crystal structures and ground-state optimized geometries

Since thermal recrystallizations of **1**, **4** and **5** from ethanol or *n*-hexane gave single-crystal samples, we performed X-ray crystallographic analyses; the crystal structures and crystallographic data are shown in Fig. S7–S9 and Table S1, respectively. The crystal structure analysis for **5** did not afford sufficient accuracy due to poor crystal quality; therefore, its crystallographic data have been omitted. The distance between the oxygen atom of the methoxy group and the nitrogen atom of the nitro group in **1** was 9.888(1) Å, and the dihedral angle between the naphthalene and phenylene rings was 51.3(2)°. The dihedral angle in **4** was slightly larger, at 60.3(3)°. These values suggest the existence of electronic interactions between the two aryl moieties in **1** and **4**, and strong charge-transfer interactions in **1**. It is worth emphasizing that two crystallographically different molecules were included in the crystal of **5** and that the nitro group in **5** stood against the naphthalene ring with dihedral angles of ~14° and ~19° for the two molecules, in contrast to the coplanar structure of **1** (~7°).

To avoid the effects of crystal packing and to compare the geometries of the six derivatives, the ground-state geometries of the molecules were optimized by DFT calculations, as shown in Fig. 1. The optimized geometries agreed with the structures obtained by crystallographic analyses. The dihedral angles between the naphthalene and phenylene (or phenyl) rings of phenylnaphthalene derivatives **1**, **2** and **4** were 55.4°–58.7°. The values arise from the steric hindrance with the hydrogen atom at the neighboring 5- (or 8-) position. In practice, biphenyl derivative **3** exhibited a smaller dihedral angle (36.5°). The nitro groups bound to the phenyl group (*i.e.*, **1**, **2**, **3** and **6**) exhibited coplanar geometries, with dihedral angles of 0.0–1.2°, and the dihedral angle between the nitro and naphthalene moieties in **5** was 27.8°, similar to that in the crystal structures. Such twisted geometry in **5** originates from the steric hindrance with the hydrogen atom at the 5-position and has a large influence on the electronic structure of the nitro group. The methoxy–nitro (O–N) distances in the biaryl derivatives **1** and **3** (9.87–9.88 Å) were larger than those of the monoaryl derivatives **5** and **6** (5.55–

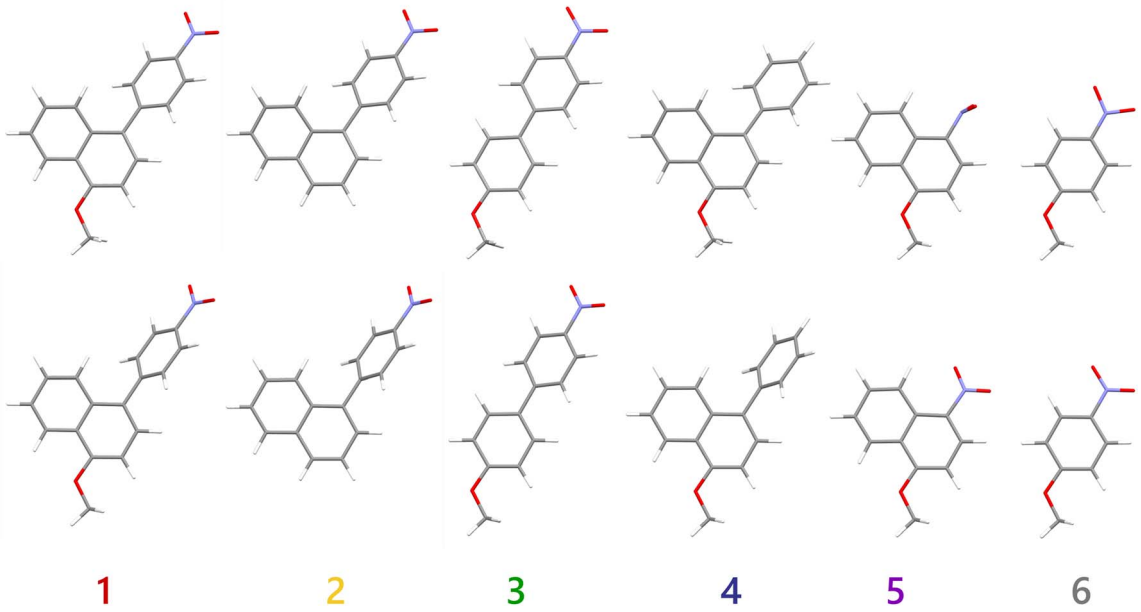

Fig. 1 Ground-state- (bottom) and S_1-optimized geometries (top) of **1–6**. Cartesian coordinates of the geometries are included in Tables S2–S7.

5.57 Å). Since large distances between the electron-donating and -withdrawing groups typically enhance the transition dipole moment and charge-transfer character in the excited state, it can be expected that **1** and **3** exhibit large fluorescent solvatochromism.

Absorption and fluorescence spectra in dichloromethane

The absorption and fluorescence spectra of **1–6** in dichloromethane at room temperature are shown in Fig. 2. All the derivatives exhibited multiple absorption bands in the measured wavelength region, and the lowest-energy absorption bands were observed at 300–370 nm. The lowest-energy bands of the derivatives were broad, suggesting the charge-transfer character. In practice, the band for **6** was much broader and lower in energy than that of benzene. The band of **1** was observed in a lower-energy region than those of the reference derivatives **2** without the methoxy group and **4** without the nitro group. Especially, the band of **4** was narrow and structured as compared with the other derivatives, indicative of a contribution of a ππ* transition in the phenylnaphthalene moiety. These results strongly suggest that the presence of the nitro group is quite important for the charge-transfer character in an electric transition and that the methoxy group extends the charge transfer. Although the band of **3** was broad and structureless, similar to that of **1**, it was higher in energy. The higher-energy absorption is explainable by the smaller π-conjugation in the linkage arylene. Derivative **5** exhibited an extremely lower-energy absorption band than expected by its small π-system. The unusual trend is presumably due to the twisted nitro–naphthalene structure as obtained by the crystallographic analysis and DFT calculations.

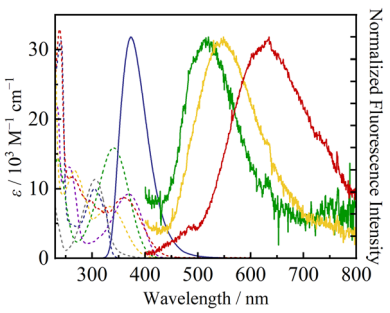

Fig. 2 Absorption (broken curves) and fluorescence spectra (solid curves) of **1** (red), **2** (yellow), **3** (green), **4** (blue), **5** (purple) and **6** (grey) in dichloromethane at room temperature.

To investigate the electronic transitions of the derivatives, TD-DFT calculations were carried out. The calculated excited states and associated molecular orbitals are given in Tables S8–S19 and Fig. S10–S15. As calculated electronic transitions agreed sufficiently with the observed absorption spectra within the accepted overestimation of the transition energies (<10%, see Fig. S16), our TD-DFT calculations reproduce the present molecules well. The lowest-energy singlet excited (S_1) states of **1–3** are best characterized by the HOMO → LUMO transitions, and they belong to charge-transfer transitions from the (methoxy)naphthalene or methoxyphenyl moiety to the nitrophenyl moiety. In contrast, the S_1 states of **4**, without the nitro group, and naphthalene derivative **5** (HOMO → LUMO for both) were mainly ascribed to the ππ* transition in the phenylnaphthalene and nitronaphthalene moieties, respectively. The ππ* character of **4** is explainable by the absence of the strong electron-withdrawing nitro group. In derivative **5**, the nitro group contributes not only to the LUMO but also to the HOMO. The contribution of the nitro group in the ground-state electronic structure is obtained for the HOMO of **6** and is presumably due to π-delocalization arising from the low-energy

π-orbital of the naphthalene or phenylene moiety. Thus, the ππ* transitions over the entire molecule (S_1 in **5** and S_2 in **6**) exhibited extremely low transition energies. The present theoretical calculations suggest that an effective intramolecular charge-transfer transition can be achieved through appropriate molecular design incorporating a 4-nitrophenyl group.

The fluorescence spectra of **1–4** in dichloromethane are shown in Fig. 2. Compounds **5** and **6** were nonemissive in various solvents. In the S_1-optimized geometry of **5** (Fig. 1), according to the TD-DFT calculations, the nitro group exhibits a non-planar structure and is oriented perpendicular to the naphthalene moiety. The perpendicular orientation reduces the orbital overlap and oscillator strength ($f = 0.0001$) in the charge-transfer transition from the methoxynaphthalene moiety to the nitro group (Tables S24, S30 and Fig. S21). The S_1 excited state of **6** also possesses a negligible f (0.0000) since the HOMO−1 localizes at the oxygen atoms on the nitro group (Tables S25, S31 and Fig. S22). Compound **4**, without the nitro group, exhibited blue fluorescence with a narrow spectral band shape and relatively small Stokes shift ($\tilde{\nu}_a - \tilde{\nu}_f = 6200\ cm^{-1}$). The spectroscopic characteristics indicate that the excited state of **4** can be ascribed to the ππ* transition in the phenylnaphthalene moiety with weak charge-transfer character from the methoxy group (supported by the TD-DFT calculations, see Tables S23, S29 and Fig. S20). On the other hand, derivatives **1–3** exhibited obvious fluorescence, despite the presence of the nitro group that often renders a derivative nonemissive. The fluorescence bands of the derivatives were broad and low-energy compared with the relevant absorption maxima, with Stokes shifts of 11 900, 11 700 and 9800 cm^{-1} for **1**, **2** and **3**, respectively. These fluorescence characteristics indicate that the excited states of the derivatives possess strong charge-transfer character. The TD-DFT calculations for the S_1-optimized geometries of **1–3** support the spectroscopic expectations, and the S_1 states of the derivatives with large charge-transfer character possess sufficiently large f values of >0.7 (Tables S20–S22, S26–S28 and Fig. S17–S19). The relatively small Stokes shift of **3**, indicating a smaller transition dipole moment for the fluorescence process, was also supported by the theoretical calculations as the HOMO of **3** in the S_1-optimized geometry is distributed over the phenylene ring in the 4-nitrophenyl group to a greater extent than those of **1** and **2**, presumably due to the similar π-energies of the two phenylene rings.

Solvent dependences of spectroscopic properties: dipole moments

Given that the charge-transfer character helps generate their excited states, it is expected that the absorption and fluorescence spectra of the derivatives are solvent-dependent. We, therefore, evaluated the solvent dependences of the spectroscopic properties of the derivatives, as shown in Fig. 3 and S23. In contrast to unclear or small solvent dependences of the absorption spectra for all the derivatives, the fluorescence color of **1–3** changed greatly when the solvent was changed. Compound **4**, without a nitro group, showed blue fluorescence, irrespective of the solvent. The details are summarized in Table 1 and described below.

Whereas the absorption band of **1** at around 360 nm was less solvent-dependent, the fluorescence maximum red-shifted greatly from 496 nm (toluene) to 672 nm (DMSO) with an increase in the solvent polarity, with a drastic color change from greenish blue to red. It is also noted that fluorescence from **1** was weak in both low- and high-polar solvents. Similar to **1**, the absorption bands at around 330 and 340 nm of **2** and **3**, respectively, were not greatly influenced by the solvent. The derivatives exhibited relatively small fluorescent solvatochromism from yellowish green (535 nm in chloroform) to orange (598 nm in acetonitrile) and from blueish green (496 nm in 1,2-dichloroethane) to yellow (565 nm in DMSO). They were almost nonfluorescent in low-polar solvents. Both the absorption and the blue fluorescence of **4**, without the nitro group, were almost solvent-independent.

The large fluorescent solvatochromism of **1–3** is expected to originate from the extensive solvent reorganization in the

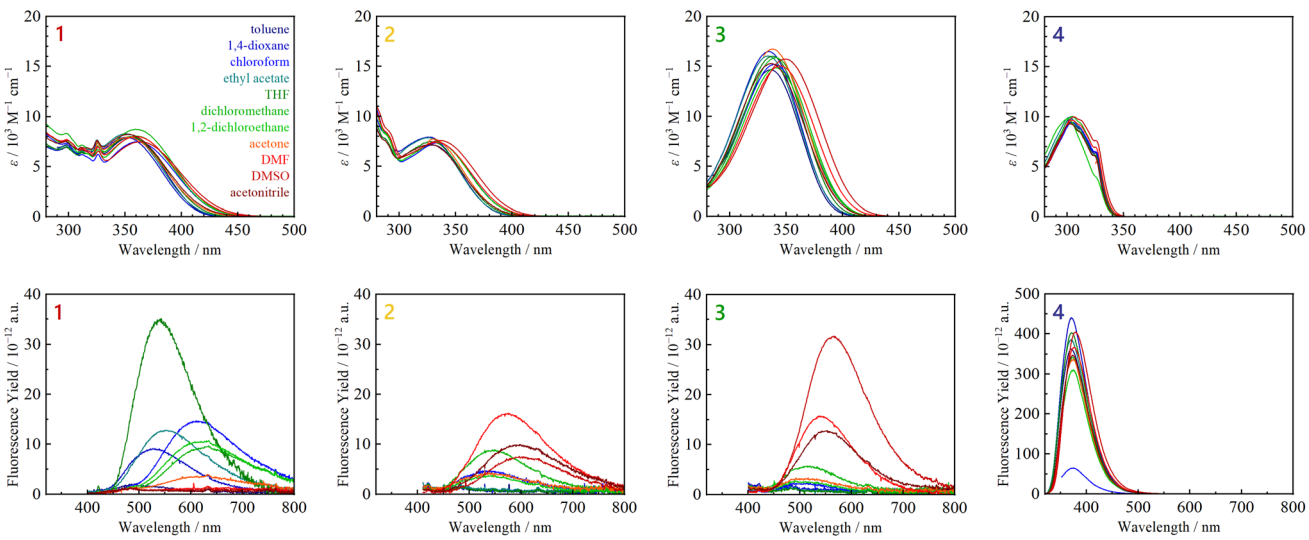

Fig. 3 Absorption (top) and fluorescence spectra (bottom) of **1–4** in various solvents.

Table 1 Solvent parameters and spectroscopic properties of **1–4**

			1		**2**		**3**		**4**	
Solvent	D_s	n	λ_a/nm	$\lambda_f{}^a$/nm ($\Phi_f{}^a$)	λ_a/nm	$\lambda_f{}^a$/nm ($\Phi_f{}^a$)	λ_a/nm	$\lambda_f{}^a$/nm ($\Phi_f{}^a$)	λ_a/nm	$\lambda_f{}^b$/nm ($\Phi_f{}^b$)
Toluene	2.379	1.49693	357	496 (0.004)	329	N.D.[c]	336	N.D.[c]	304	371 (0.23)
1,4-Dioxane	2.209	1.42241	352	530 (0.01)	326	N.D.[c]	334	N.D.[c]	303	370 (0.28)
Chloroform	4.806	1.44590	362	610 (0.03)	334	535 (0.008)	340	502 (0.003)	304	374 (0.04)
Ethyl acetate	6.053	1.37239	351	550 (0.02)	326	N.D.[c]	334	N.D.[c]	302	374 (0.25)
THF	7.580	1.40716	356	541 (0.05)	328	N.D.[c]	338	N.D.[c]	303	372 (0.26)
Dichloromethane	8.930	1.42416	360	629 (0.02)	333	545 (0.02)	341	512 (0.009)	304	375 (0.22)
1,2-Dichloroethane	10.37	1.44480	360	614 (0.02)	334	539 (0.007)	341	496 (0.004)	303	374 (0.18)
Acetone	20.70	1.35868	352	621 (0.008)	330	544 (0.008)	338	508 (0.006)	N.D.[d]	377 (0.20)
DMF	36.71	1.43047	360	654 (0.005)	334	572 (0.03)	345	540 (0.02)	305	377 (0.24)
DMSO	46.45	1.47930	365	672 (0.004)	336	595 (0.01)	350	565 (0.05)	306	379 (0.27)
Acetonitrile	35.94	1.34411	353	671 (0.003)	327	598 (0.02)	338	550 (0.02)	303	373 (0.22)

[a] λ_{ex} = 375 nm. [b] λ_{ex} = 300 or 340 nm. [c] Could not be determined. [d] Could not be determined due to overlap with solvent absorption.

excited state owing to their large charge-transfer character. We, thus, estimated the electric dipole moments in the excited (μ_e) and ground states (μ_g) by using the absorption/fluorescence maximum energies and solvent polarity parameters $f(D_s,n)$ and $g(n)$ in eqn (2),[25] where D_s and n are the relative permittivity and refractive index of the solvent,[19] respectively.

$$f(D_s,n) = \frac{2n^2+1}{n^2+2}\left[\frac{D_s-1}{D_s+2} - \frac{n^2-1}{n^2+2}\right] \quad (2a)$$

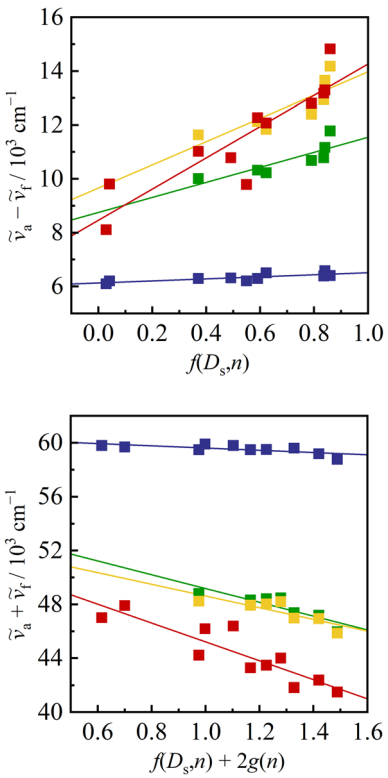

Fig. 4 Solvent-parameter dependences of the spectroscopic properties of **1–4**. The colors correspond to those indicated in Fig. 2. Solid lines correspond to the linear regressions.

$$g(n) = \frac{3}{2}\left[\frac{n^4-1}{(n^2+2)^2}\right] \quad (2b)$$

As shown in Fig. 4, the difference and sum of absorption ($\tilde{\nu}_a$) and fluorescence maximum energies ($\tilde{\nu}_f$) exhibited good linear relationships against $f(D_s,n)$ and $[f(D_s,n) + 2g(n)]$, respectively. The results indicate that the fluorescence changes of the derivatives originate from the solvent polarity. Thus, the electric dipole moments of the derivatives in the excited and ground states were successfully estimated from the slopes of the linear regressions (m_1 and m_2) using eqn (3):

$$\mu_e = \frac{m_2+m_1}{2}\sqrt{\frac{hca_O}{2m_1}} \quad (3a)$$

$$\mu_g = \frac{m_2-m_1}{2}\sqrt{\frac{hca_O}{2m_1}} \quad (3b)$$

where h and c are the Planck constant and the speed of light, respectively, and a_O is the Onsager radius of a molecule using values obtained from optimized geometries by the DFT calculations (Table 2). Compounds **1–3**, with nitro groups, possess large excited-state dipole moments of 7.4–10 D ($D = 10^{-18}$ esu cm), and the excited state of **1** is largely charge-separated. Large μ_e values were also obtained by the TD-DFT calculations for the S_1-optimized geometries (8.86, 8.12 and 9.48 D for **1**, **2** and **3**, respectively). The origin of the largest μ_e of **1** is explained as

Table 2 Solvent–dependent parameters (m_1 and m_2) and excited- and ground-state electric dipole moments of **1–4**

Derivative	a_O/Å	m_1/cm^{-1}	$-m_2$/cm^{-1}	μ_e/D	μ_g/D
1	5.33	5800 ± 9700	7000 ± 1200	+10 ± 0.9	+1.0 ± 2.0
2	5.01	4300 ± 1300	4300 ± 1300	+7.4 ± 1.3	0.0 ± 2.6
3	4.96	2800 ± 8400	5100 ± 1300	+8.2 ± 1.1	+2.4 ± 3.1
4	5.24	0830 ± 1000	0380 ± 1000	+3.7 ± 0.8	+1.4 ± 1.5

follows. The π-orbital of the naphthalene moiety and the non-bonding orbital of the methoxy group efficiently mix owing to their small energy gap, and the large contribution of the methoxy group enhances the charge-transfer distance. In practice, the HOMO of **1** in the S_1-optimized geometry distributes more extensively onto the methoxy group than in the case of **3** (Tables S26 and S28, Fig. S17 and S19).

Energy gap plot for solvent dependence

In the course of the solvent-dependent measurements, we noticed unusual solvent responses of the derivatives: the fluorescence from **1** was weak in both low- and high-polar solvents, and compounds **2** and **3** were weakly fluorescent in low-polar solvents. A charge-transfer excited state is typically more stabilized in polar solvents and, in the resulting low-energy excited state, thermal deactivation to the ground state is accelerated as expressed by the famous energy gap law.[26–28] A similar unusual solvent response was also reported by Konishi and coworkers, who noted that 2-methoxy-6-(4-nitrophenyl)naphthalene, an isomer of **1**, and its derivatives exhibited the most intense fluorescence when the fluorescence maximum was ~580 nm.[13] To elucidate the origin of such unusual solvent dependences, we evaluated the energy gap dependence of nonfluorescence rates for the solvent dependence of **1–3**. As shown in the fluorescence decay profiles of **1–3** (Fig. S24–S26), although many fluorescence decay profiles could be fitted with a single exponential decay function, several samples required a bi-exponential decay function due to their weak and short-lived fluorescence competing with the time resolution of our system. At this stage, intensity-weighted average lifetimes ($\langle\tau_f\rangle = \Sigma(A_i\tau_i^2)/\Sigma(A_i\tau_i)$) were employed for the biexponential fluorescence decays. It is also noted that, although the fluorescence lifetimes of some solutions in the present study were short and competing with our instrumental response, the τ_f values were successfully determined by deconvoluting the instrumental response function (*e.g.*, $\tau_f = 15$ ps with a standard deviation of 0.15 ps for **1** in acetonitrile).

Fluorescence (k_f) and nonfluorescence rate constants (k_d), calculated by the equation $\Phi_f = k_f\tau_f = k_f/(k_f + k_d)$, where k_d is the sum of rate constants of the internal conversion from S_1 state to the ground state (k_{ic}) and the intersystem crossing to the triplet excited state (k_{isc}), are summarized in Table 3 together with the fluorescence lifetimes. Both Φ_f (in Table 1) and τ_f values of **1** were largest in THF (with moderate polarity) and decreased with both increasing and decreasing solvent polarity. Those of **2** and **3** were the largest in high-polar solvent (**2** in DMF and **3** in DMSO) and decreased with a decrease in the solvent polarity. The k_f values of **1** were larger than its isomer as reported by Konishi and coworkers.[13] The result is explained by the larger transition dipole moment (typically $k_f \approx A|\mu_e|^2$) by linearly bound methoxy–nitro substituents to the bridging arylene. Although the solvent dependences of the k_f values of the derivatives are not clear, the values seem to be larger in the high-polar solvent by a factor of ≤4. On the other hand, the k_d values of the derivatives were highly solvent-dependent, especially for **1** (*e.g.*, 6.8×10^{10} s^{-1} in acetonitrile and 1.1×10^9 s^{-1} in ethyl acetate and THF), and there is no doubt that the value determines the Φ_f and τ_f of the derivatives. Although the solvent dependences of the k_d of **2** and **3** were less clear compared to that of **1** due to smaller change in the fluorescence energy arising from smaller dipole moments in the excited states and due to fluorescence energies of **2** locating at the valley of the energy gap plot (*vide infra*), the tendency is explainable by

Table 3 Solvent dependence of the photophysical properties of **1–3**

Derivative	Solvent	$\tau_f{}^a$/ps	$k_f{}^b/10^7$ s^{-1}	$k_d{}^b/10^9$ s^{-1}
1	Toluene	70	5.2	15
	1,4-Dioxane	97 (90%) 330 (10%)	8.8	6.0
	Chloroform	390	7.4	2.5
	Ethyl acetate	870	2.6	1.1
	THF	830	5.9	1.1
	Dichloromethane	280	7.2	3.5
	1,2-Dichloroethane	350	6.3	2.8
	Acetone	130	6.2	7.4
	DMF	36	13	28
	DMSO	26	15	38
	Acetonitrile	15	20	68
2	Chloroform	270 (52%) 620 (48%)	1.5	1.9
	Dichloromethane	300 (29%) 530 (71%)	3.1	2.0
	1,2-Dichloroethane	290 (93%) 720 (7%)	1.9	2.8
	Acetone	82 (61%) 250 (39%)	4.0	5.1
	DMF	1100	2.8	0.90
	DMSO	500	2.9	2.0
	Acetonitrile	350	5.7	2.8
3	Chloroform	120	2.8	8.2
	Dichloromethane	100	9.0	10
	1,2-Dichloroethane	73 (92%) 200 (8%)	4.4	10
	Acetone	80	7.3	13
	DMF	390	5.7	2.5
	DMSO	510	9.7	1.9
	Acetonitrile	260	7.9	3.8

[a] $\lambda_{ex} = 380$ nm. [b] $\Phi_f = k_f\tau_f = k_f/(k_f + k_d)$.

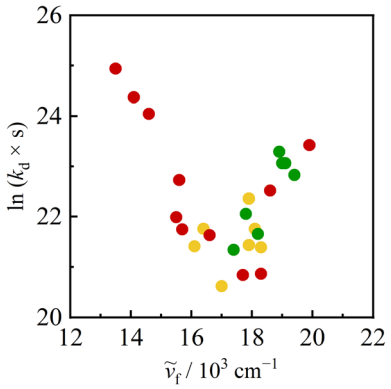

Fig. 5 Energy gap plots for **1–3**. The colors correspond to those indicated in Fig. 2.

integrating the data for **1–3**. Fig. 5 shows plots for the k_d of **1–3** against the fluorescence maximum energy ($\tilde{\nu}_f$). The energy gap plots of the three derivatives in various solvents exhibited an identical trend, suggesting that the fluorescent S_1 states of the derivatives were lost *via* similar pathways. It is, furthermore, worth noting that the energy gap dependence exhibited a two-step behavior that switched at $\tilde{\nu}_f \approx 17\,000$ cm^{-1}. In the region below 17 000 cm^{-1}, ln k_d linearly decreased with increasing $\tilde{\nu}_f$ (coefficient of determination $R^2 = 0.92887$), following the energy gap law. The behavior originates from the internal conversion from the S_1 state to the ground state. On the other hand, in the region >17 000-cm^{-1}, ln k_d increased with $\tilde{\nu}_f$ ($R^2 = 0.70198$). To explain such reverse energy gap dependence, a contribution from another nonfluorescent state, for example, intersystem crossing to the triplet excited state, is required.

To experimentally observe the contribution of another nonfluorescent state in the high $\tilde{\nu}_f$ region, we performed transient absorption measurements for **1** in toluene ($\tilde{\nu}_f = 19\,900$ cm^{-1}) and acetonitrile ($\tilde{\nu}_f = 13\,500$ cm^{-1}), whose k_d are large nevertheless they are located at the high- and low-energy regions, respectively, in the energy gap plot. The transient absorption spectra of **1** in toluene (Fig. 6(a)) exhibited a broad absorption band at >430 nm, whereas that in acetonitrile (Fig. 6(b)) was silent. The transient absorption signal in toluene decayed with a microsecond timescale (Fig. 6(c)), and the decay time constant was determined to be 1.4 μs. The value is much longer than the fluorescence lifetime ($\tau_f = 70$ ps) and is, therefore, clear evidence of the existence of another state contributing to the excited-state dynamics of **1** in the high $\tilde{\nu}_f$ region. A similar transient absorption signal with a lifetime of 4.6 μs was also observed for **2** in toluene (Fig. S27), whose fluorescence was not detectable in spite of the high-energy excited state expected on the basis of the polarity of toluene. Since the lifetimes of the other nonemitting (dark) states of **1** and **2** are on the microsecond timescale and the spectral features are similar to each other, we expect that they are the triplet excited states with a charge-transfer character in the (4-nitrophenyl)naphthalene skeleton. Transient absorption measurement for **3** in acetonitrile ($\tilde{\nu}_f = 17\,800$ cm^{-1}) also gave a broad signal with a 4.8-μs decay constant (Fig. S28). Although the k_d of **3** in acetonitrile is small among the present solutions, the observation of the transient signal is not unusual due to its slow internal conversion process. The present transient absorption measurements detect the lowest-energy triplet excited (T_1) state and, therefore, the transient absorption spectrum of **3** with a different spectral feature from those of **1** and **2** does not explain the identical reverse energy gap dependence of **1–3** by direct intersystem crossing to the T_1 state. By comparing the triplet excited states of the derivatives in the S_1-optimized geometries by TD-DFT calculations (Tables S20–S22, S26–S28 and Fig. S17–S19), the second triplet excited state (T_2 state) of **1–3** possesses comparable energies of 2.45 ± 0.03 eV (equal to 19 800 cm^{-1}). The T_2 state was, furthermore, solvent-independent, as summarized in Tables S32–S34. The T_2 states of the three derivatives were ascribed to the charge-transfer transition from the nitro group to a 4-nitrophenyl moiety (see Fig. S29–S31). On the basis of these results, we modeled the excited-state dynamics of a derivative with a 4-nitrophenyl group, as shown in Fig. 7. When the fluorescence energy of the derivative is lower than 17 000 cm^{-1}, the internal conversion (IC) from the fluorescent S_1 state to the ground (S_0) state is accelerated with a decrease in the excited-state energy, as

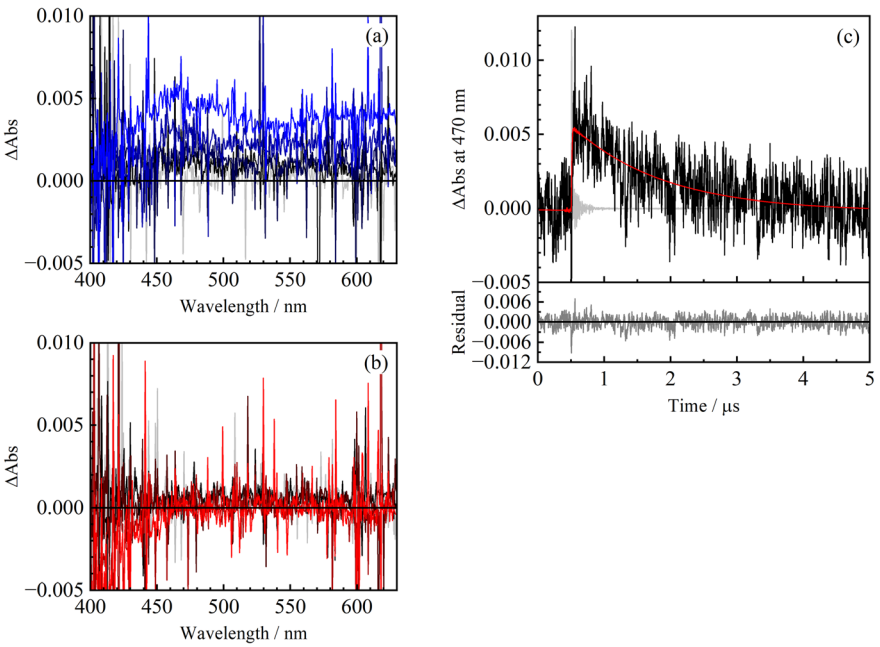

Fig. 6 Transient absorption spectra of **1** in (a) toluene (6×10^{-5} M) and (b) acetonitrile (5×10^{-5} M) at 50, 500, 1000 and 2000 ns (blue or red to black) after the 355-nm excitation and (c) transient absorption decay profile at 470 nm of **1** in toluene (black, 6×10^{-5} M). The grey and red curves in (c) represent the instrumental response function and convolution fit by the single exponential decay function, respectively.

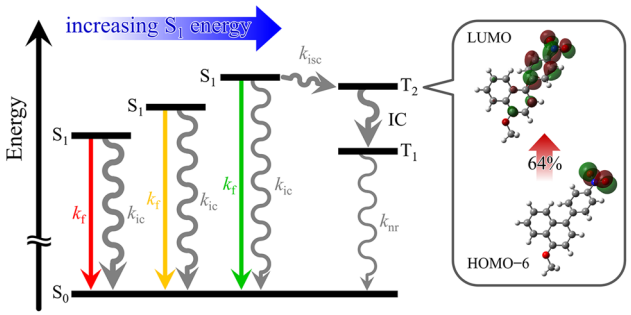

Fig. 7 Plausible excited-state processes of a derivative with a 4-nitrophenyl group.

expressed by the energy gap law. On the other hand, the intersystem crossing (ISC) from the S_1 state to the T_2 state increases its contribution with increasing S_1-state energy, and the ISC process dominates the excited-state dynamics of a derivative in the region of the fluorescence energy >17 000 cm^{-1}. The generated T_2 state is quickly converted into the T_1 state, which is observed by the transient absorption measurements, by IC, followed by the thermal deactivation to the S_0 state. The existence of two nonfluorescence processes gives the V-shape energy gap dependence of derivatives with a 4-nitrophenyl group, and most derivatives with a nitro group(s) are nonfluorescent due to the narrow window of $\tilde{\nu}_f$ with small k_d (17 000 ± 1000 cm^{-1}).

Conclusions

A novel fluorescent naphthalene derivative with 4-nitrophenyl and methoxy groups (**1**) and its analogues were synthesized, and their spectroscopic/photophysical properties, including solvent dependences, were studied in detail. Dilute solutions of **1** exhibited obvious, broad, and low-energy absorption/fluorescence ascribed to the charge-transfer transition from the methoxy group to the 4-nitrophenyl group. Compound **1** and the two reference derivatives, **2** and **3**, showed fluorescent solvatochromism. In particular, the fluorescence color of **1** varied significantly from greenish blue to red, depending on the solvent. The solvent-dependent spectroscopic study revealed that the excited-state electric dipole moment of **1** was the highest among the derivatives in the present study. The presence of the nitro group induces a charge-transfer character in the electronic transition, and the introduction of the methoxy group extends the charge transfer. The bridging arylene structure is also important for the efficient charge transfer. The fluorescent solvatochromic derivatives (**1**, **2** and **3**) exhibited unusual solvent dependences of their photophysical properties: weak and short-lived fluorescence for **1** in both low- and high-polar solvents and for **2** and **3** in low-polar solvents. The energy gap plot for the nonfluorescence rate constant (k_d) of the derivatives in various solvents exhibited a two-step behavior that switched at a fluorescence energy of ~17 000 cm^{-1}. When the fluorescence from the derivative was higher in energy than 17 000 cm^{-1}, ln k_d linearly increased with the fluorescence energy, whereas it decreased in the low-energy region as expressed by the energy gap law. The transient absorption measurements and TD-DFT calculations revealed that the reverse energy gap dependence in the high-energy region originates from the increasing contribution of the intersystem crossing to a triplet excited state localized in the 4-nitrophenyl moiety. Owing to the narrow, small-k_d window arising from the V-shape energy gap dependence, most derivatives with a nitro group are known to be nonemissive. It is expected that each nitroaryl group (*e.g.*, 4-nitrophenyl, 4-nitropyridyl and so forth) possesses a characteristic triplet-state energy that is insensitive to other chemical structures. Appropriate molecular design by tuning the fluorescence energy and selecting a 4-nitroaryl group in terms of experimental and/or theoretical investigations will open the door to the development of fluorescent molecules with a nitro group(s).

Author contributions

Conceptualization: M. M. and A. I.; syntheses and characterization: M. M.; spectroscopic and photophysical measurements/analyses: M. M. and A. I.; single-crystal XRD analyses: A. I.; writing–original draft: M. M.; and writing–review and editing: M. M. and A. I.

Conflicts of interest

There are no conflicts to declare.

Data availability

The data supporting this article have been included as part of the supplementary information (SI). Supplementary information (SI): ^{1}H NMR spectra and DFT/TD-DFT calculations of the derivatives; crystallographic data for **1**, **4** and **5**; solvent dependences of absorption spectra of **5** and **6**; fluorescence decay profiles of **1**–**3**; and transient absorption data of **2** and **3**. See DOI: https://doi.org/10.1039/d5ra07359f.

CCDC 2491387 and 2491388 contain the supplementary crystallographic data for this paper (**1** and **4**).[29a,b]

Acknowledgements

MM acknowledges JST-SPRING (JPMJSP2141) for the financial support.

References

1 I. S. Park, M. Yang, H. Shibata, N. Amanokura and T. Yasuda, *Adv. Mater.*, 2022, **34**, e2107951.
2 W. Z. Yuan, Y. Gong, S. Chen, X. Y. Shen, J. W. Y. Lam, P. Lu, Y. Lu, Z. Wang, R. Hu, N. Xie, H. S. Kwok, Y. Zhang, J. Z. Sun and B. Z. Tang, *Chem. Mater.*, 2012, **24**, 1518–1528.
3 V. Rubio, N. McInchak, G. Fernandez, D. Benavides, D. Herrera, C. Jimenez, H. Mesa, J. Meade, Q. Zhang and M. J. Stawikowski, *Sci. Rep.*, 2024, **14**, 30777.

4 K. Yan, Z. Hu, P. Yu, Z. He, Y. Chen, J. Chen, H. Sun, S. Wang and F. Zhang, *Nat. Commun.*, 2024, **15**, 2593.
5 S. K. Patra, R. Manivannan and Y.-A. Son, *Dyes Pigm.*, 2025, **233**, 112534.
6 A. Ito, K. Kawanishi, E. Sakuda and N. Kitamura, *Chem.–Eur. J.*, 2014, **20**, 3940–3953.
7 Y. Niko, S. Kawauchi and G. Konishi, *Chem.–Eur. J.*, 2013, **19**, 9760–9765.
8 E. Sakuda, Y. Ando, A. Ito and N. Kitamura, *J. Phys. Chem. A*, 2010, **114**, 9144–9150.
9 C. Hansch, A. Leo and R. W. Taft, *Chem. Rev.*, 1991, **91**, 165–195.
10 A. Ito, Y. Kuroda, K. Iwai, S. Yokoyama and N. Nishiwaki, *RSC Adv.*, 2024, **14**, 5846–5850.
11 M. C. Chen, D. G. Chen and P.-T. Chou, *ChemPlusChem*, 2021, **86**, 11–27.
12 Y. M. Poronik, G. V. Baryshnikov, I. Deperasinska, E. M. Espinoza, J. A. Clark, H. Agren, D. T. Gryko and V. I. Vullev, *Commun. Chem.*, 2020, **3**, 190.
13 S. Hachiya, K. Asai and G.-i. Konishi, *Tetrahedron Lett.*, 2013, **54**, 1839–1841.
14 O. V. Dolomanov, L. J. Bourhis, R. J. Gildea, J. A. K. Howard and H. Puschmann, *J. Appl. Crystallogr.*, 2009, **42**, 339–341.
15 G. M. Sheldrick, *Acta Crystallogr., Sect. A:Found. Adv.*, 2015, **A71**, 3–8.
16 G. M. Sheldrick, *Acta Crystallogr., Sect. C:Struct. Chem.*, 2015, **C71**, 3–8.
17 B. N. Briggs, F. Durola, D. R. McMillin and J.-P. Sauvage, *Can. J. Chem.*, 2011, **89**, 98–103.
18 B. List and D. Höfler, *Synlett*, 2021, **33**, 38–39.
19 M. Montalti, A. Credi, L. Prodi and M. T. Gandolfi, *Handbook of Photochemistry*, Taloy & Francis CRC Press, Oxon, U. K., 3rd edn, 2006.
20 M. J. Frisch, G. W. Trucks, H. B. Schlegel, G. E. Scuseria, M. A. Robb, J. R. Cheeseman, G. Scalmani, V. Barone, G. A. Petersson, H. Nakatsuji, X. Li, M. Caricato, A. V. Marenich, J. Bloino, B. G. Janesko, R. Gomperts, B. Mennucci, H. P. Hratchian, J. V. Ortiz, A. F. Izmaylov, J. L. Sonnenberg, D. Williams-Young, F. Ding, F. Lipparini, F. Egidi, J. Goings, B. Peng, A. Petrone, T. Henderson, D. Ranasinghe, V. G. Zakrzewski, J. Gao, N. Rega, G. Zheng, W. Liang, M. Hada, M. Ehara, K. Toyota, R. Fukuda, J. Hasegawa, M. Ishida, T. Nakajima, Y. Honda, O. Kitao, H. Nakai, T. Vreven, K. Throssell, J. A. Jr, J. E. Peralta, F. Ogliaro, M. J. Bearpark, J. J. Heyd, E. N. Brothers, K. N. Kudin, V. N. Staroverov, T. A. Keith, R. Kobayashi, J. Normand, K. Raghavachari, A. P. Rendell, J. C. Burant, S. S. Iyengar, J. Tomasi, M. Cossi, J. M. Millam, M. Klene, C. Adamo, R. Cammi, J. W. Ochterski, R. L. Martin, K. Morokuma, O. Farkas, J. B. Foresman, and D. J. Fox, *Gaussian 16, Revision A.03*, Gaussian, Inc., Wallingford, CT, 2016.
21 A. D. Becke, *J. Chem. Phys.*, 1993, **98**, 5648–5652.
22 P. J. Hay and W. R. Wadt, *J. Chem. Phys.*, 1985, **82**, 299–310.
23 V. Barone and M. Co, *J. Phys. Chem. A*, 1998, **102**, 1995–2001.
24 R. Dennington, T. A. Keith and J. M. Millam, *GaussView, Version 6.0.16*, Semichem Inc., Shawnee Mission, KS, 2016.
25 J. R. Mannekutla, B. G. Mulimani and S. R. Inamdar, *Spectrochim. Acta, Part A*, 2008, **69**, 419–426.
26 R. Englman and J. Jortner, *Mol. Phys.*, 1970, **18**, 145–164.
27 S.-H. Son, Y. Abe, M. Yuasa, Y. Yamagishi, N. Sakai, T. Ayabe and K. Yamada, *Chem. Lett.*, 2011, **40**, 378–380.
28 H. A. Z. Sabek, A. M. M. Alazaly, D. Salah, H. S. Abdel-Samad, M. A. Ismail and A. A. Abdel-Shafi, *RSC Adv.*, 2020, **10**, 43459–43471.
29 (*a*) CCDC 2491387: Experimental Crystal Structure Determination2025DOI: **10.5517/ccdc.csd.cc2pmhb5**; (*b*) CCDC 2491388: Experimental Crystal Structure Determination2025DOI: **10.5517/ccdc.csd.cc2pmhc6**.